Chapter

Unsteady Aerodynamics of Highly Maneuvering Flyers

Mohamed Yehia Zakaria

Abstract

In this chapter, a set of analytical aerodynamic models, based on potential flow, that can be used to predict the unsteady lift response during pitching maneuvers are presented and assessed. The result examines the unsteady lift coefficients experienced by a flat plate in high-amplitude pitch ramp motion. The pitch ramps are chosen based on two ramp pitch maneuvers of a maximum amplitudes of 25 and 45 degrees starting from zero degree. The aim is investigate the use of such classical models in predicting the lift dynamics compared to a full physical-based model. Among all classical methods used, the unsteady vortex lattice method (without considering the leading edge vortex) is found to be a very good predictor of the motion lift dynamic response for the 25° ramp angle case. However, at high pitch maneuvers (i.e.,the 45° ramp angle case), could preserve the response pattern with attenuated amplitudes without high computational burden. These mathematical analytical models presented in this chapter can be used to obtain a fast estimate for aircraft unsteady lift during pitch maneuvers instead of high fidelity models, especially in the early design phases.

Keywords: canonical maneuvers, pitching maneuvers, unsteady aerodynamics, unsteady lift response

1. Introduction

Loops, barrel rolls and pitch maneuvers are impressive aerial stunts. But even during the most intense in-air aerobatics, most planes are still constrained by aerodynamics. The air flowing over their wings gives them the lift to stay aloft and they control their movement by altering the surfaces that air flows over. The quick the rate of movement for the control surface, a fast response from the aircraft to change attitude. Pilots can pull off moves with precise control in conditions that would leave other aircraft hopelessly plummeting towards the ground. For fighter aircraft, there are numerous maneuvers can be done by the pilot to increase the aircraft maneuverability. These maneuvers such as, Cobra, Mango flip, high pass alpha that can save pilot's life during a dog fight (see **Figure 1**). Nowadays, unmanned aeriel vehicles autopilots can perform these maneuvers to an extent. Consequently, in order assure that UAVs could perform such maneuvers, one may need to relax the quasi-steady modeling to an unsteady nonlinear model to deal with these abrupt changes in attitude. Prediction of dynamic lift response of Harsh maneuvers for flying vehicles necessitate a compact aerodynamic modeling. For instance, pitching

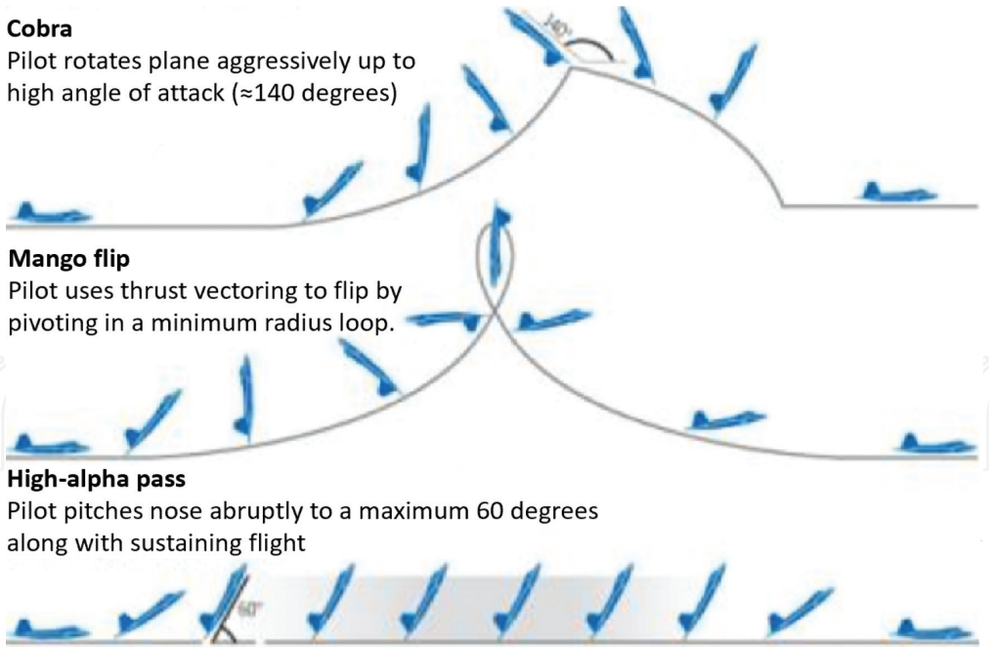

Figure 1.
High alpha Fighter's aircraft maneuvers.

maneuvers for fighter aircrafts (ex. F35 - SU-57) with specified handling qualities stimulate the idea to impose new modeling techniques to be applied on UAVs. The unsteady lift response plays an important role to control the vehicle at such low speeds. Escaping from a flying threat, first performed by Soviet test pilot Viktor Pugachoyov in 1989, the maneuver that would go on to be called "Pugachev's Cobra" is one of the building blocks that makes up many other more complicated supermaneuvers. During flight, the pilot pulls back to an absurd angle of attack, taking the nose of the aircraft completely vertical or even beyond. From here, one of two things can happen. In a plane without thrust vectoring but with a thrust-to-weight ratio higher than one, the drag towards the tail of the plane can be used to pitch the nose forward again. If the plane does have thrust vectoring, that can help the re-orientation even more. But either way, the engines are firing hard enough the entire time to maintain the jet's altitude despite the loss of speed and lift.

After few years, a German test pilot Karl-Heinz Lang performed the Herbst Maneuver in 1993. The Herbst Maneuver is basically Pugachev's Cobra with a bit of a twist. Instead of just pulling up and going forward again, the Herbst Maneuver has the pilot roll the plane (experimental X-31) a bit while its nose is pointed at the sky, so that when the nose comes back down, the plane is pointed in a different direction. On the other hand, such maneuvers are also possessed by birds and flapping insects. They can twist their wings at high angles of attack while flapping their wings without approaching stall. This is known as non-conventional lifting mechanisms invoked from biomemetics in order to perform such maneuver with a stabilized flight (i.e. vibrational stabilization). In preliminary design of UAVs, potential flow models are used as a start point to ensure acceptable estimates for aerodynamic forces and moments. A recent motivation is devoted towards designing flight control systems that can achieve harsh maneuvers such as perching and sudden landing for fixed wing MAV's [1, 2]. Bird perching is considered one of the most fascinating landing and decelerating maneuvers. **Figure 2(a)** shows a tailed swallow feeding a chick by pitching its wing at high angle of attack. For specific missions, such maneuver is useful for both flapping-wing and fixed-wing MAVs.

For classical unsteady aerodynamic models, Theodorsen [5], Wagner [6] and others have been studied extensively the classical theories of unsteady aerodynamics to be employed in the aeroelasticity field. However, aerodynamic models of harsh maneuvers characterized by sharp pitch rates and amplitudes still present a challenge in modeling. While advances in computational fluid dynamics and experimental methods have opened the study of these maneuvers as such a low-fidelity analytical modeling for rigorous prediction is still forthcoming. Roderich et al. [4] performed experiments for touchdown to take-off for a very basic glider as shown in **Figure 2(b)**.

In the last two decades, there have been several efforts exerted on unsteady aerodynamic modeling based on potential flow theories as well as modified thin airfoil theory to simulate the wing motion for an arbitrary input [7, 8]. The AIAA Fluid Dynamics Technical Committee's (FDTC) Low Reynolds Number Discussion Group introduced some cases for the assessment of experimental efforts [9], on large amplitude pitching maneuvers. The proposed motions are used as a benchmark for obtaining analytical and phenomenological models, in which a ramp up, hold, and ramp-down motions are analyzed using theory and numerical computations [10–14] Theodorsen's and Wagner's Inviscid theories are purely proper only for small amplitude oscillations associated with planar wakes. However, a tremendous work has shown that these methods remain substantially accurate even at moderate amplitudes and high frequencies. The results obtained by Ramesh et al. [9] during the hold and downstroke show that the aerodynamic forces are dominated by a deep-stall as well as leading edge vortex (LEV). The shedding effects were seen from the vorticity and dye injection plots from his experimental results. These results proved that viscous state indicate that the inviscid assumptions are insufficient for modeling the hold and downstroke portions of the motion and adequate for capturing the lift time history during the ramp phase.

A tremendous work was done based on nonlinear unsteady reduced order modeling to solve flow at high frequencies [8, 15–19]. The recent work done by Yuelong et al. [20] examined the unsteady forces and moment coefficients obtained by a thin airfoil in a pitch ramp high-amplitude motion. Wind tunnel experiments have been conducted at Reynolds number ($Re = 45 \times 10^4$), using a rigid flat-plate

(a) (b)

Figure 2.
Example of bird perching and successful experiments based on perching manoeuver. (a) A wire-tailed swallow feeding a re-cently edged chick [3] (a) A wire-tailed swallow feeding a re-cently edged chick [3]. (b) A basic glider, manually thrown and con-trolled by perching [4].

model. Forces have been measured for reduced pitch rates ranging from 0.01 to 0.18 reduced frequency ($k = \omega c/2U_\infty$) along with four maximum pitch angles (30°; 45°; 60°; 90°) at different pivot axis locations. The results show that the unsteady aerodynamics is limited to a delayed stall effect for reduced pitch rates lower than k = 0.03. At higher pitch rates, the unsteady aerodynamic response is associated with a formation of circulation, which in turn increases with the pitch rate and the distance between the pivot axis and the 3/4-chord location. An enhanced response was noted in the normal force and moment coefficients due to these circulatory effects. These overshot is slightly reduced for a flat plate with a finite aspect ratio near eight compared to two-dimensional configuration. The authors proposed a new time-dependent model for both lift and moment coefficients. The model based on the Wagner function and a time-varying input along with nonlinear variation of the quasi steady aerodynamics. A satisfactory results for 0° to 90° pitch ramp motions were compared with experiments for different pivot locations and various circulation intensity based on pitch rates.

On the other hand, fluid structure interaction modeling became essential for solving flow around vibrating and rotating structure [8, 21–23]. Modeling such moving bodies requires aerodynamic unsteady nonlinear models to assure accuracy in modeling results rather than using quazi-steady models. Carlos et al. [24] work discuses modeling and analyzing procedures of the non-linearities induced by the flow-structure interaction of an energy harvester consisting of a laminated beam integrated with a piezoelectric sensor. The cantilevered beam and the piezoelectric lamina are modeled using a nonlinear finite element approach, while unsteady aerodynamic effects are described by a state-space model that allows for arbitrary nonlinear lift characteristics.

The major contribution about the classical unsteady formulations discussed in the literature is the inefficacy to account for a non-conventional lift curve, such as LEV effects and dynamic stall contributions. Taha et al. [7] developed a state space model that captures the nonlinear contributions of the LEV in an unsteady fashion. However, their underpinning dynamics is linear: convolution with Wagner's step response. Consequently, there is a considerable gap in the literature for consolidating low fidelity models for predicting accurate lift forces associated with these large-amplitude maneuvers. An analytical unsteady nonlinear aerodynamic model that can be used to characterize the local and global nonlinear dynamic characteristics of the airflow is a mandatory task for aerodynamicists. Developing such a model will be indispensable for multidisciplinary applications (e.g., dynamics, control and aeroelasticity).

The chapter investigates and assesses relevant classical analytical models in solving lift response for pitching maneuovers. In doing so, Theodorsen, Wagner and Unsteady vortex lattice methods are used to predict the lift dynamics, then the results are compared with the experimental data presented by Ramesh et al. [9]. Also, the work proposed a simple time-dependent model in order to predict the lift response for a two dimensional wing performing rapid pitch motion. In addition, the results provide a comparison with numerical simulation using the unsteady vortex lattice method. The aerodynamic system receives the time histories of angle of attack, quasi-steady lift as inputs and produces the corresponding total unsteady lift as output. In the following sections, each presented model will be explained in detail. The chapter is organized as follows. The adopted motion kinematics are presented in Section 2. Aerodynamic classical models are reported in Section 3, along with the effect of reduced pitch rate and pivot axis location. In Section 4, the effect of pitch amplitudes on the unsteady lift coefficient is investigated by comparing the obtained results using two different pitch amplitudes with the experimental results [9].

2. Motion kinematics

In order to explore the non-periodic motions of wings rapid manouevers, the ramp-hold-return motions were proposed by the AIAA FDTC Low Reynolds Number Discussion Group [25]. The smoothed ramp motion proposed by Eldredge's canonical formulation [12] is used in this work as a reference case for comparison. Here, the experimental work done by Ramesh et al. [13] is considered as a benchmark. Variations of this motion are considered by varying the pitch amplitude (25° and 45°) at a Reynolds number of 10,000. **Figures 2** and **3** show a schematic of the pitch motion variables and the two studied maneuvers versus the non-dimensional time, respectively. **Figure 4** shows the ramped motion for a maximum amplitude of 25° versus the corresponding effective angle of attack and the local angle of attack at the 3/4 chord location as suggested by Pistolesi theorem [26].

To avoid any numerical instabilities, (e.g., dirac-delta function spikes in the calculation of the added mass force) all motions are smoothed based on a smoothing parameter introduced by Elderedge [12]. For a ramp going from 0 degrees angle of attack to 25 or 45 degrees, the first 10% (2.5 or 4.5 degrees) can be replaced with a sinusoidal tangent to the baseline ramp, and similarly in approaching the "hold" portion at the maximum amplitude angle of attack, consequently again on the downstroke. This treatment avoids a piece-wise linear fit which has discontinuities in the angle derivatives. The smoothing function G(t) is defined as:

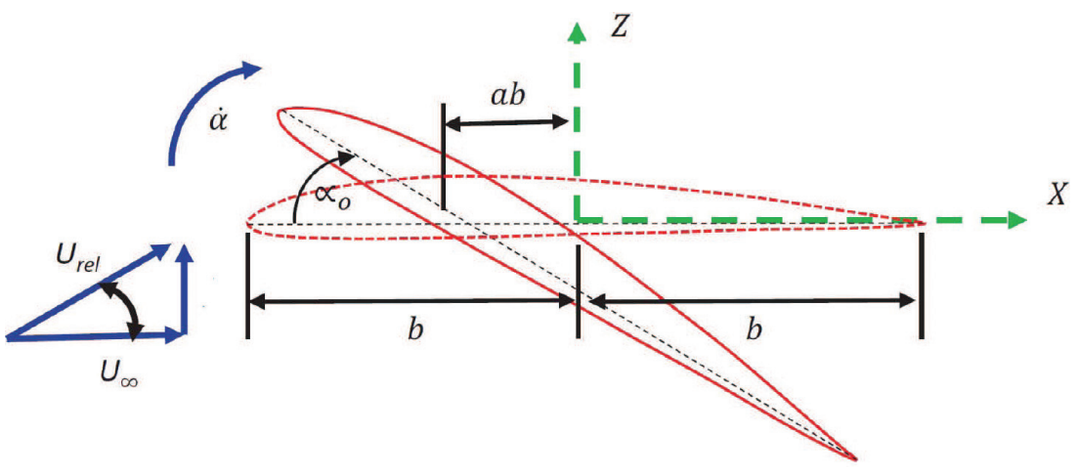

Figure 3.
Pitching motion nomenclature and motion variables (a = 1 is the leading edge pivot, a = 0 is the mid chord pivot and a = −1 is trailing edge pivot).

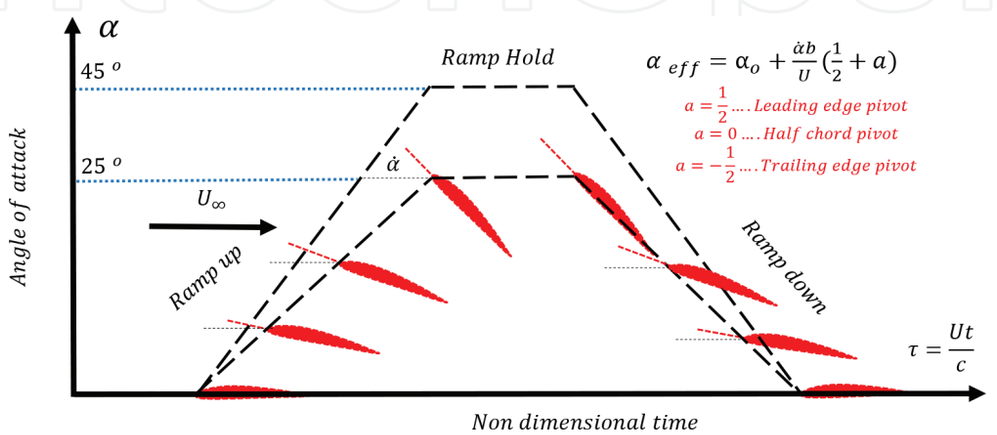

Figure 4.
The proposed ramp maneuver with a maximum amplitudes of 25° and 45° and pitch rates of 0.2 and 0.4, respectively.

$$G(t) = ln\left(\frac{cosh\left(aU_\infty(t-t_1)/c\right)cosh\left(aU_\infty(t-t_4)/c\right)}{cosh\left(aU_\infty(t-t_1)/c\right)cosh\left(aU_\infty(t-t_4)/c\right)}\right) \quad (1)$$

where a is the smoothing parameter and is taken to be 11, t_1 through t_4 are the transition times and a pitch amplitude angle A. As such, the smoothed angle of attack can be written as:

$$\alpha(t) = A\frac{G(t)}{max\left(G(t)\right)} \quad (2)$$

3. Classical models

In order to analytically describe the generated lift force due to pitching maneuvers, a well established models were introduced. In this section, a detailed description of these models is discussed and explained in a straight forward manner.

3.1 Theodorsen model

The tremendous work done by Wagner [6], Prandtl [27], Theodorsen [28] and Garrick [29] described some fundamental physical concepts in understanding and modeling the unsteady aerodynamics. These concepts are usually incorporated with a potential flow approach and small disturbance theory to obtain analytical expressions of flow quantities. The unsteady lift on a harmonically oscillating airfoil in incompressible flow has been studied by Kussner and Schwarz [30], but the most well known solution is due to Theodorsen [5]. The lift on a thin rigid airfoil undergoing oscillatory motion can be written as:

$$L = \underbrace{\pi\rho b^2\left(\ddot{h} + U_\infty\dot{\alpha} + ba\ddot{\alpha}\right)}_{Added\ \ mass} + \underbrace{2\pi\rho U_\infty b\left(\dot{h} + U_\infty\alpha + b\left(\frac{1}{2}+a\right)\dot{\alpha}\right)}_{Quasi\ \ steady}C(k) \quad (3)$$

or in normalized form,

$$C_L = \frac{\pi b}{U_\infty^2}\left(\ddot{h} + U_\infty\dot{\alpha} + ba\ddot{\alpha}\right) + 2\pi C(k)\left(\frac{\dot{h}}{U_\infty} + \alpha + b\left(\frac{1}{2}+a\frac{\dot{\alpha}}{U_\infty}\right)\right) \quad (4)$$

where, $\ddot{h}$ and $\ddot{\alpha}$ are plunging and pitching accelerations respectively. The first group of terms are the noncirculatory components which account for the inertia of fluid (added mass force). The second group of terms are the circulatory components, where C(k) accounts for the influence of the shed wake vorticity (lift deficiency factor). Since Theodorsen function necessitates a periodic motion for its input parameters (e.g. angle of attack or quasi steady lift), a Fourier transform should be applied to the pitch ramp maneuver under study. The effective angle of attack of the proposed ramp pitch motion can be written as:

$$\alpha_{eff} = \alpha + \dot{\alpha}\left(\frac{1}{2}+a\right)\frac{b}{U_\infty} \quad (5)$$

Two approaches were undertaken to test the transformed input functions for Theodorsen classical unsteady model as follows:

- Fourier series approach

By applying Fourier series for the given effective maneuver angle of attack and considering Theodorsen function C(k) such that:

$$A_{c(k)} = |C(k)|, and\ \phi = \angle(C(k)) \tag{6}$$

where $A_{c(k)}$ is the absolute value (amplitude) and ϕ is the phase angle. The circulatory lift given after applying Fourier series is given by:

$$L_{Circ} = \pi\rho U^2 c a_o + \rho U^2 c\left(A_{C(k)}\right)(a_n \cos(\omega t + \phi) + b_n \sin(\omega t + \phi)) \tag{7}$$

The non-circulatory lift part [31] is given by:

$$L_{Non-Circ} = -\pi\rho b^2[U\dot{\alpha} + \ddot{\alpha}ab] \tag{8}$$

- Fast Fourier transform

The Fast Fourier Transform of the effective angle of attack is written as:

$$\alpha_{eff}(\omega) = \int_0^\infty \alpha_{eff}(t)e^{-i\omega t}dt \tag{9}$$

and the circulatory component of lift based on FFT is given by:

$$L_{Circ-FFT} = \frac{1}{2}\rho U^2 c\int_{-\infty}^{\infty} \alpha_{eff}(w)C(k)e^{i\omega t}d\omega \tag{10}$$

It should be noted that practically, this Fourier transform approach will be implemented numerically using discrete fourier transform. However, discrete Fourier transform in contrast with the exact Fourier transform (Fourier integral) will necessarily ignore some frequency contents due to the integration limits between $-\infty$ to $+\infty$.

3.2 Wagner step response and Duhamel superposition principle

Using Wagner's linear step response, the Duhamel principle can be used to include the unsteady effects in an exact form such as a finite-state aerodynamic models suitable for aeroelastic problems and flight mechanics simulations. Wagner [6] obtained the time dependant-response of the lift on a flat plate due to a step input (indicial response problem). Garrick [29] showed that by using Fourier transformation, Wagner function, $W(s)$, and Theodorsen function, $C(k)$ can be related together. Wagner [6] determined the circulatory lift due to a step change in the wing motion. The unsteady lift is then written in terms of the static lift as:

$$\ell(s) = \ell_s W(s) \tag{11}$$

where the non-dimensional time S is defined as $S = \frac{2U_\infty t}{c}$ for constant free-stream velocity U_∞.

By knowing the indicial response for a linear dynamical system, the response due to arbitrary motion (input) can be described as an integral (superposition)

using the indicial response and an input varies with time. The variation of the circulatory lift for an arbitrary change in the angle of attack is given by:

$$\ell(s) = \pi\rho U^2 c\left(\alpha(0)W(s) + \int_0^s \frac{d\alpha(\sigma)}{d\sigma} W(s-\sigma)d\sigma\right) \tag{12}$$

We note that $W(s)$ can also be used as an indicial response to aerodynamic inputs other than the angle of attack. Van der Wall and Leishman [32] used it as an indicial response to the wing normal velocity, $w = U\alpha$, in the case of time-varying free stream. For a relatively high angle of attack, the Duhamel superposition is performed using a more exact normal velocity $w = U\sin\alpha$. Eq. (11) is then re-written as

$$\ell(s) = \pi\rho U(s) c\left(U(0)\sin\alpha(0)W(s) + \int_0^s \frac{d(U(\sigma)\sin\alpha(\sigma))}{d\sigma} W(s-\sigma)d\sigma\right) \tag{13}$$

This equation is usually used in dynamic stall models where relatively high angles of attack are encountered, e.g., the Beddoes-Leishman dynamic stall model [33].

3.3 State space finite model

RT Jones proposed an approximate expression for Wagner function as follows:

$$\phi(s) = 1 - A_1 e^{-c_1 s} - A_2 e^{-c_2 s} \tag{14}$$

where $A_1 = 0.165, A_2 = 0.335, c_1 = 0.0455, c_2 = 0.3$ and s is the reduced time parameter and is given by $U_\infty t/b$. By taking the Laplace transform with an operator P:

$$\phi(P) = \frac{1}{P} - \frac{A_1}{P + \frac{c_1 U_\infty}{b}} - \frac{A_2}{P + \frac{c_3 U_\infty}{b}} \tag{15}$$

the transfer function is then written as:

$$G(P) = \frac{Y(P)}{\alpha_{eff}(P)} = \frac{\phi(P)}{1/P} = 1 - \frac{A_1\ P}{P + \frac{c_1 U_\infty}{b}} - \frac{A_2 P}{P + \frac{c_2 U_\infty}{b}} \tag{16}$$

$$G(P) = \frac{\left(P + \frac{c_1 U_\infty}{b}\right)\left(P + \frac{c_2 U_\infty}{b}\right) - A_1 P\left(P + \frac{c_2 U_\infty}{b}\right) - A_2 P\left(P + \frac{c_1 U_\infty}{b}\right)}{\left(P + \frac{c_1 U_\infty}{b}\right)\left(P + \frac{c_2 U_\infty}{b}\right)} \tag{17}$$

$$G(P) = \frac{(1 - A_1 - A_2)P^2 + \left(\frac{c_1 U}{b}(1 - A_2) + \frac{c_2 U}{b}(1 - A_1)\right)P + \frac{c_1 c_2 U^2}{b^2}}{P^2 + (c_1 + c_2)\frac{UP}{b} + \frac{c_1 c_2 U^2}{b^2}} \tag{18}$$

To determine a second-order state-space realization of the transfer function in Eq. 17 can be written as:

$$\frac{Y}{\alpha_{eff}} = \frac{b_2 P^2 + b_1 P + b_0}{P^2 + a_1 P + a_0} = \frac{Y}{X}\frac{X}{\alpha_{eff}} \tag{19}$$

where X is the internal states of the system, which is related to the input via these coefficients $a_o = \frac{(C_1+C_2)U_\infty}{b}$, $a_1 = \frac{(C_1 C_2)U_\infty^2}{b^2}$, $b_o = \frac{(C_1 C_2)U_\infty^2}{b^2}$, $b_1 = \left(\frac{C_1 U_\infty}{b} + \frac{C_2 U_\infty}{b} - \frac{A_1 C_2 U_\infty}{b} - \frac{A_2 C_1 U_\infty}{b}\right)$, $b_2 = 1 - A_1 - A_2$ as follows:

$$\frac{X}{\alpha_{eff}} = \frac{1}{P^2 + a_1 P + a_0} \tag{20}$$

$$\frac{Y}{X} = \frac{b_2 P^2 + b_1 P + b_0}{1} \tag{21}$$

and to the output via:

$$XP^2 + Xa_1 P + Xa_0 = \alpha_{eff} \tag{22}$$

then applying Laplace inverse we get:

$$\ddot{X} + a_1 \dot{X} + a_o X = \alpha_{eff} \tag{23}$$

then let $X_1 = X$ and $X_2 = \dot{X}$.
Also,

$$Y = Xb_2 P^2 + Xb_1 P + b_0 X = b_2 \ddot{X} + b_1 \dot{X} + b_o X \tag{24}$$

Hence,

$$Y = b_2 \left(\alpha_{eff} - a_o X_1 - a_1 X_2\right) + b_1 X_2 + b_o X_1 \tag{25}$$

By writing these equation in a matrix form, we obtain

$$\frac{d}{dt}\begin{pmatrix} X_1 \\ X_2 \end{pmatrix} = \begin{bmatrix} 0 & 1 \\ -a_o & -a_1 \end{bmatrix}\begin{pmatrix} X_1 \\ X_2 \end{pmatrix} + \begin{pmatrix} 0 \\ 1 \end{pmatrix}\alpha_{eff} \tag{26}$$

$$y = [b_o - b_2 a_o \; b_1 - b_2 a_1]\begin{pmatrix} X_1 \\ X_2 \end{pmatrix} + (b_2)\alpha_{eff} \tag{27}$$

then by applying the quasi-steady lift expression, we have;

$$L_{QS} = \rho U_\infty \Gamma = 2\pi\rho U_\infty b \, W_{3/4} \tag{28}$$

where $W_{3/4}$ is the normal velocity component and is given by:

$$\begin{aligned} W_{3/4} &= U_\infty \sin(\alpha) + \dot{\alpha}\left[\frac{b}{2} + a\right] \\ L_c(t) &= 2\pi\rho U_\infty b[\, b_o - b_2 a_o \; b_1 - b_2 a_1 \,]\begin{pmatrix} X_1 \\ X_2 \end{pmatrix} + [b_2] W_{3/4} \end{aligned} \tag{29}$$

3.4 Unsteady vortex lattice method (UVLM)

The unsteady Vortex lattice methods (UVLMs) are well suited to the bio-inspired flight problems because they can account for the circulation distribution variations on wings, the velocity potential time-dependency, and the shedding of wake downstream. Although they are considered low fidelity models, they may be extended to capture unconventional lift mechanisms such as leading edge vortex [34–36]. These discrete vortex models are widely used in modeling aerodynamics of aircraft and rotorcraft analysis, compared to computational fluid dynamics (CFD) models which are more computationally expensive [37]. The use of UVLM method

is now a powerfull tool in hand for aerodynamicists for its ease implementation even for complex shapes.

Zakaria et al. [8] used UVLM to model the aerodynamic loading on different Samara leaves (Maple seeds) during their steady state flight. The results were verified with experiments. Parameters including the drop speed, angular velocity and coning angle for different sets of Maple Samaras were determined from experiments. The aerodynamic loads were calculated using UVLM against the forces required for maintaining a steady state flight as obtained from the experiment. Consequently, the UVLM approach yields adequate aerodynamic modeling features that can be used for more accurate flight stability analysis of the Samara flight or of decelerator devices inspired by such flight. Also, Simon et al. [38] showed that by imposing an arbitrary input as a control surface deflection to an unsteady VLM suitable for efficient aerodynamic loads analysis within aeroelastic modeling, analysis and optimization frameworks for preliminary aircraft design. By using a continuous time state space aerodynamic model is extended for accepting arbitrary motion, control surface deflection and gust velocities as inputs. Their results showed good agreement for a large range of reduced frequencies. Accepting arbitrary motion, control surface deflection and gust velocities as inputs.

The (UVLM) divides the lifting surface into panels. A point vortex is then associated with each of these panels. The center of this ring is set at the 1/4 of the panel chord length. One collocation point is set in each panel at the 3/4 of the panel length, and the panel normal vector is calculated in this point as shown in **Figure 5**.

The UVLM model is based on the following assumptions:

- No penetration boundary condition.
- Kelvin Circulation Theorem (Conservation of Circulation).
- Vortices is convected by local velocities. (Wake deformation)

The velocity induced by all the vortex points, including the shed vorticies through the wake, is calculated at each control point and the no-penetration kinematic boundary condition is applied to calculate vortex intensity on each panel. At each time step, there are (m + 1) unknowns (m $\gamma_{boundvortices}$'s and $\gamma_{atrailingedgevortex}$), then (m + 1) equations are needed for closure. For the no-penetration boundary condition at m control points, we have:

$$V_{cp}^{(n)} = V_{air}^{(n)}\Big|_{cp} \tag{30}$$

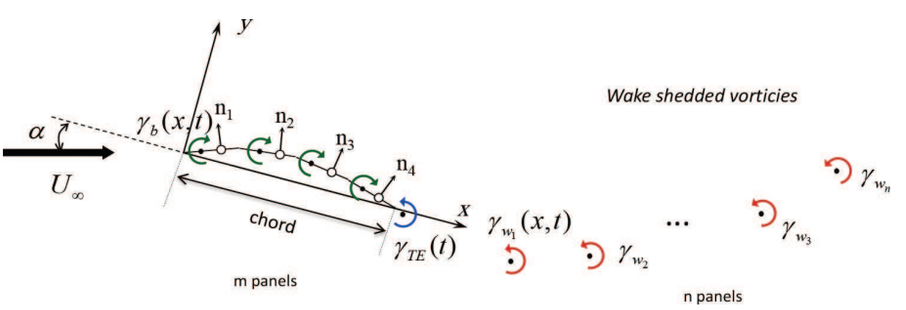

Figure 5.
A schematic diagram showing the panels on the airfoil camber and the shedded vortices used in UVLM modeling.

From Kelvin's circulation theorem, we have:

$$\sum \Gamma_{tot} = \sum \gamma_b + \gamma_w = 0 \Rightarrow \sum \gamma_b + \gamma_{TE} = -\Gamma_w \tag{31}$$

where Γ_w is the sum of all wake vortices, which are know from previous time steps. As such, we obtain the following linear system,

$$\begin{pmatrix} a_{1,1} & a_{1,2} & \dots & a_{1,MN} \\ a_{2,1} & a_{2,2} & \dots & a_{2,MN} \\ \vdots & \vdots & \ddots & \vdots \\ a_{MN,1} & a_{MN,2} & \dots & a_{MN,MN} \end{pmatrix} \begin{Bmatrix} \Gamma_1 \\ \Gamma_2 \\ \vdots \\ \Gamma_{MN} \end{Bmatrix} = \begin{Bmatrix} RHS_1 \\ RHS_2 \\ \vdots \\ RHS_{MN} \end{Bmatrix}, \tag{32}$$

where a_{K_1,K_2} are the influence coefficients from the point vortex K_2 at the control point K_1 and it is equal to the normal velocity that the point vortex induces at the control point $\Gamma_{K_2} = 1$. Each element on the right hand side is $RHS_K = -\left(\vec{v} + \vec{v}_w\right)_K \cdot \vec{n}_K$, where $\vec{v}$ is the wind flow velocity relative to the surface and $\vec{v}_w$ is the velocity induced at the control point K by all the other vortex point in the wake created before the time t. In order to satisfy the unsteady Kutta condition, the wake is created at each instant of time at the trailing edge by shedding a new vortex that has an intensity equal to the bound vortex on the panel along the trailing edge. At each instant of time all the points in the wake generated in previous steps are convected downstream following the induced velocity generated by all the vortices on the surface and through the wake. The velocity induced by each vortex is computed by using the Biot Savart law. This induced velocity is inversely proportional to the distance between the vortex location and the control point where the velocity is calculated. Having solved the linear system [39] in the bound vorticity, the pressure difference through the bound vortex sheet is computed based on the unsteady Bernoulli's equation. More details can be found in [40].

The unsteady aerodynamic loads can be calculated from the circulation Γ_K of the K^{th} panel and its time rate of change [40]. Using the unsteady Bernoulli equation,

$$\frac{\Delta P(x)}{\frac{1}{2}\rho U_\infty^2} = \rho\left(\frac{d}{dt}\int_0^c \gamma_b(x)dx + U_\infty \gamma_b(x)\right) \tag{33}$$

the unsteady pressure difference on the K^{th} panel is given by,

$$\left(\frac{p_l - p_u}{\rho}\right)_K = \left(\frac{\Delta p}{\rho}\right)_K = \left(\frac{V_u^2 - V_l^2}{2}\right)_K + \left(\frac{\partial \phi_u}{\partial t}\right)_K - \left(\frac{\partial \phi_l}{\partial t}\right)_K, \tag{34}$$

where p denotes the static pressure, V is the tangent velocity, ϕ is the velocity potential, and the subscripts u and l are used to represent the upper and lower surfaces, respectively.

From the definition of circulation, we have:

$$\left(\frac{\partial \phi_u}{\partial t}\right)_K - \left(\frac{\partial \phi_l}{\partial t}\right)_K = \frac{\partial \Gamma_{i,j}}{\partial t} = \frac{\Gamma_{i,j}(t) - \Gamma_{i,j}(t-1)}{\Delta t}, \tag{35}$$

for i = 1, 2, ..., M, and by applying the Kutta-Joukowski theorem, the normal force on each panel is obtained from:

$$\vec{F}_{N_K} = -(\Delta p \Delta S)_{i,j} \vec{n}_{i,j} \quad , \tag{36}$$

where ΔS is the area of each panel.

3.5 Models comparison

In order to summarize the merit of the proposed classical potential models for solving high pitch maneuvers, **Table 1** is shown. **Table 1** represents the key parameters for each model in the sense of input motion, nonlinearity, wake deformation and camber variation for flying vehicles. The merit of each model is how one can apply simple analytical equation to solve such maneuver.

4. Maneuver case studies results

4.1 Case 1: Pitch ramp $\alpha_o = 25^o$

4.1.1 Leading edge pivot

Figures 6–11 show a comparison between the proposed models discussed above for different ramp amplitudes and hinge locations. A physical interpretation for the jump and attenuated lift peaks show four flow events as reported by Ramesh et al. [9] as follows: (i) onset of flow separation at the ramp start ($\tau = 1$), (ii) the formation of a leading edge vortex ($\tau = 1 - 3$), (iii) ramp hold ($\tau = 3 - 4$) and (iv) detachment of the leading-edge vortex ($\tau = 4 - 6$).

Figure 6 shows the ramp pitch motion with an amplitude of 25^o about a leading edge hinge. Almost all the theoretical models have the same jump during the transition of each event start and end positions during the whole ramp manoeuver compared to the experimental results. During upstroke, $\tau = 1 - 3$, a very good match is found between the experimental results and the UVLM results. The prediction of the quasi-steady model is higher compared to the experimental results which is expected as it lacks the dynamics of the flow and is based only the static behavior of the generated lift. On the other hand, all other presented models show an attenuated lift response during the ramp-up phase. During the ramp hold period, $\tau = 3 - 4$, a very good agreement between all the models and the experiments except the quasi-steady and Theodorsen FFT based model. During the ramp-down phase, the UVLM model matches very well with the experimental results preserving the lift dynamics. On the other hand, all models over predict the lift coefficient except the quazi-steady model shows a lower lift coefficient. As reported by Yu et al. [14], the reason for this discrepancy could be attributed to the sensitivity of these models to capture the LEV de-attachment and the lift decrease during this phase. Based on the observations of Ramesh et al. [9], this behavior points to an

Models	Input motion	Nonlinearity	wake deformation	Camber variation
Theodorsen	Harmonic	Geometric	Flat	×
Wagner	Step input	Geometric	×	×
State space	Arbitrary	×	×	×
UVLM	Arbitrary	√	√	√

Table 1.
Classical aerodynamics proposed models for solving pitching maneuvers.

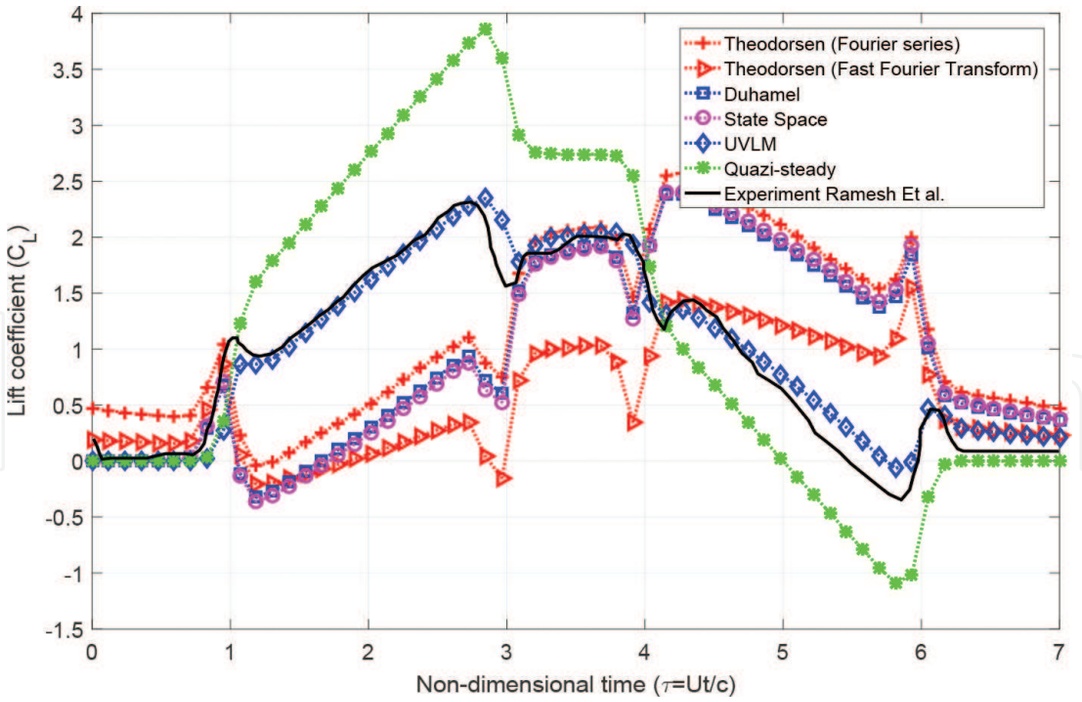

Figure 6.
Comparison for the proposed models and experimental work done by Ramesh et al. with ramp rate of 0.2 and amplitude 25° at the leading edge hinge location.

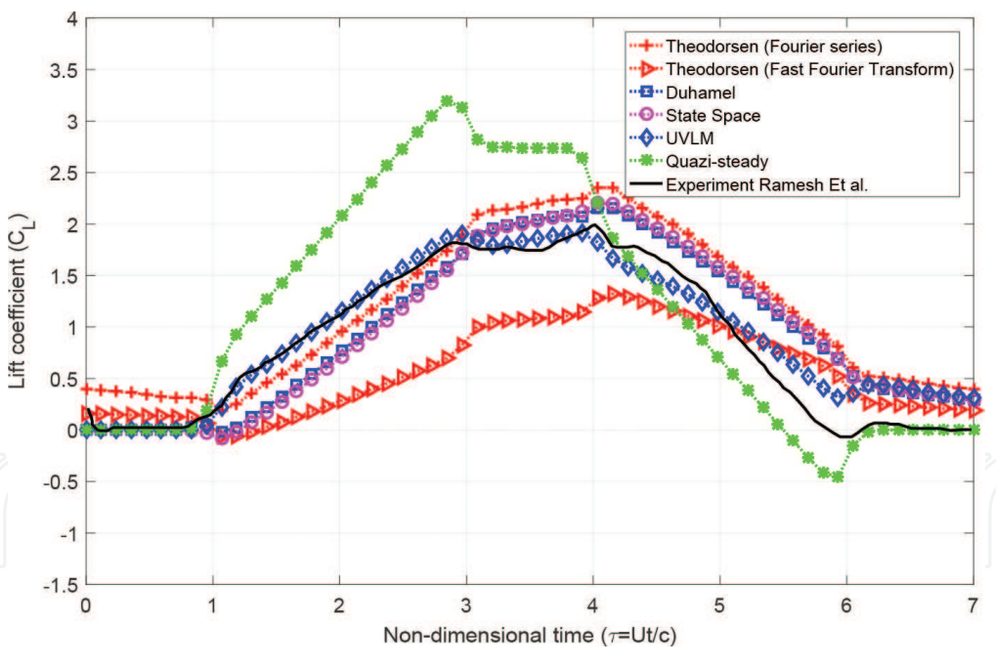

Figure 7.
Comparison for the proposed models and experimental work done by Ramesh et al. with ramp rate of 0.2 and amplitude 25° at the half chord hinge location.

important aspect, where the lift dynamics results in a considerable delay; i.e. the lift response does not depend on the past history (memory effects).

4.1.2 Half chord pivot

Figure 7 shows the ramp with amplitude of 25^{o} at the mid chord hinge location. The results show a good agreement with the experimental results by having the same lift response slope except for Thoedorsen model based on FFT model

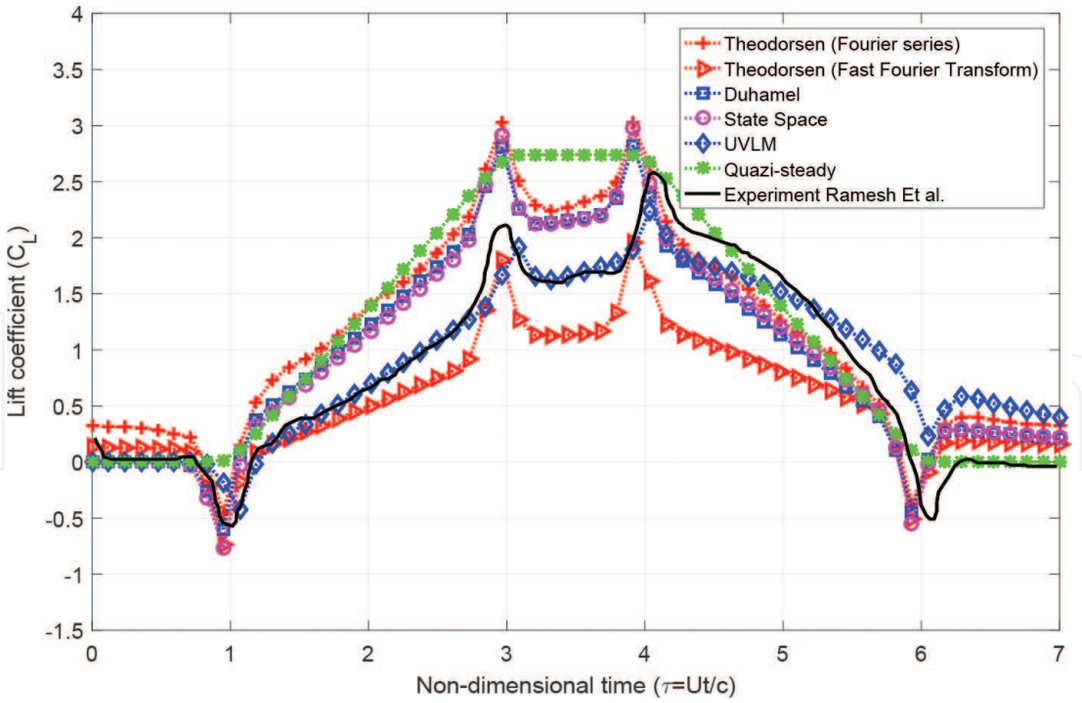

Figure 8.
Comparison for the proposed models and experimental work done by Ramesh et al. with ramp rate of 0.2 and amplitude 25° at the leading edge hinge location.

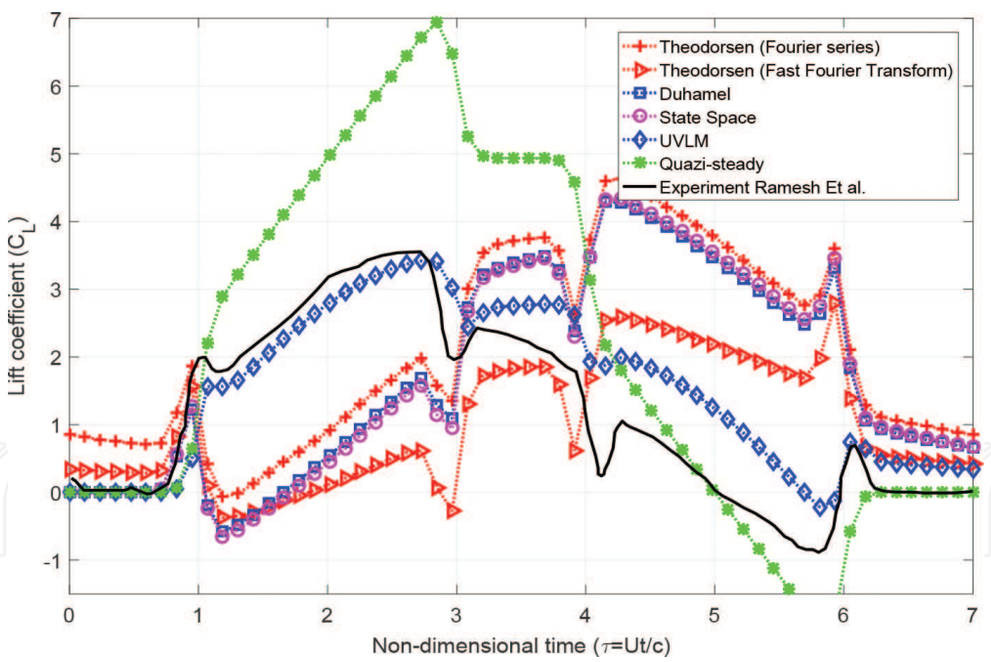

Figure 9.
Comparison for the proposed models and experimental work done by Ramesh et al. with ramp rate of 0.4 and amplitude 45° at leading pivot location.

(attenuated response) and the quasi-steady model (over predicted). Of particular interest, Duhamel and state space models coincide on top of each other having the same lift magnitude. This is excepted as the two models have the same mathematical base. At the ramp hold phase, the value of the saturated lift coefficient is approximately 2 for all models except the quasi-steady and Theodorsen based on FFT. Here, the impact of shifting the pivot location towards the trailing edge conducive in reducing the rotational effects which in turn decreases the lift coefficient by 15% at the ramp-up event compared to the quarter chord location. This

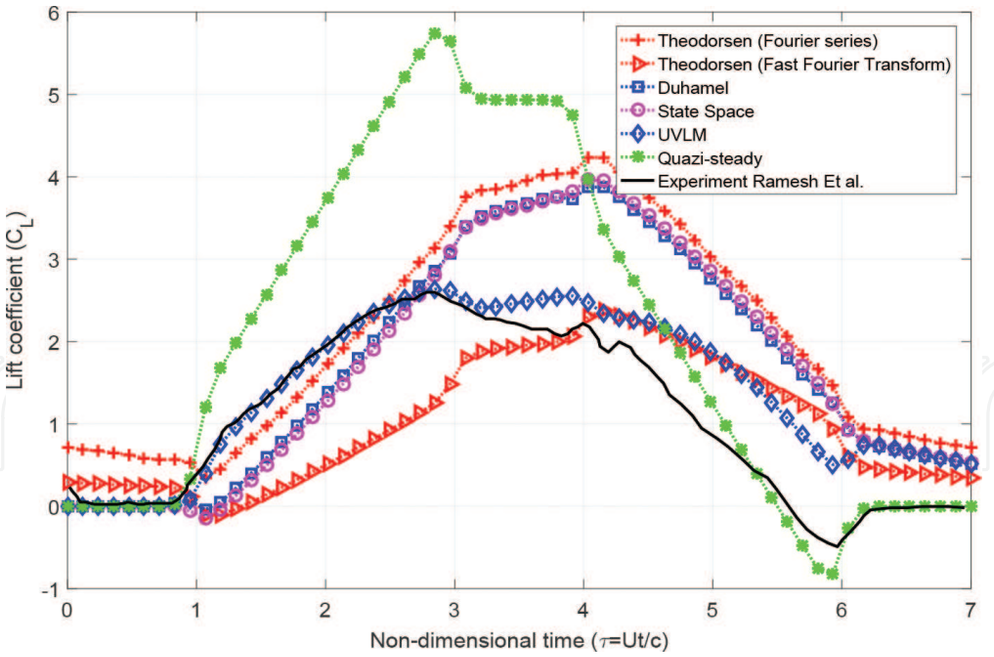

Figure 10.
Comparison for the proposed models and experimental work done by Ramesh et al. with ramp rate of 0.4 and amplitude 45° at half chord pivot location.

conclusion was reported also by Yu et al. [14] in their recent work for examining the effect of pivot locations on force and moment coefficients.

4.1.3 Trailing edge pivot

In a similar manner, **Figure 8** shows a comparison between experimental and theoretical predictions for 25^o ramp case pitched about the trailing edge pivot. Lift coefficient comparison shows a qualitatively good agreement between the experiment and all the presented models (lift coefficient pattern). Of particular interest, taking the lift transition peaks during different ramp regimes. UVLM model results match very well for the ramp-up and ramp-hold regimes then decrease slightly at the ramp-down regime to give an damped lift coefficient values. Theodorsen model based on Fast Fourier Transform records an attenuated lift coefficient compared to experiments. On the other hand, all other presented models show an over predicted lift coefficient compared to the experimental results while preserving the same lift response pattern for all ramp regimes.

The common result in all pivot location cases (leading, half and trailing chord location), show that Theodorsen FFT model has a damped lift response compared to all the proposed models and experiments. This is because for a given AOA (α), one could be interested in the transient response, however, the analytical expressions cannot be obtained and the discrete Fourier Transform (FFT) has to be used instead. Discrete Fourier Transform compared to the exact Fourier Transform ignores some frequency content mathematically. In addition to the aside notion of flow dynamics, the leading edge location experiences rich dynamics when compared to the half and trailing pivot chord locations reported by Ford and Babinsky [41]. This is due to the inclusion of rotational effects which increase by increasing the spacing between the hinge point and the three-quarter chord location. It is clear that all models capture the lift peaks during transition between pitch ramps except the quasi-steady model. This lift peak has been reported by previous studies due to a delay in stall and/or a delay in LEV formation [39, 42].

4.2 Case 1: Pitch ramp $\alpha_o = 45^o$

4.2.1 Leading edge pivot

Figures 9–11 show the lift coefficient response for a ramp maneuver with an amplitude of 45^o at three different pivot locations. At the leading edge pivot location; shown in **Figure 8**, at the beginning of the ramp ($\tau = 0 - 1$), Theodorsen model based on Fourier series model shows higher lift coefficient than all the other models as well as the experimental results. For the ramp upstroke, all the models showed a decrease in the lift coefficient compared to the experiment results preserving the same slope until the start of the second event then a continuous increase in lift response which appears as over predicted values compared to the experimental results presented by Ramesh et al. [9]. The UVLM model pertained the same lift pattern and all proposed models show a large discrepancy compared to experimental results. In addition, the UVLM model results show a good agreement with experiments at the ramp-up then starts to deviate with an increase in lift coefficient by 48% at hold-on and ramp down regimes. Furthermore, the quasi steady model shows a high lift coefficient at the end of the ramp-upstroke compared to the experiments, followed by a sharp decrease at the ramp-down stroke.

4.2.2 Half chord pivot

Figure 10 shows the lift coefficient for a ramp amplitude of 45^o at half chord pivot location. The proposed models show a good match at the ramp-up regime then an over predicted lift coefficient occurs after the ramp-hold and ramp-down regimes compared to the experimental results except for Theodorsen FFT based model and the quasi-steady model. Again, Theodorsen FFT based model gives an attenuated response, and the quasi-steady model shows a magnified response (qualitatively similar to the results presented in **Figure 7** of a pitch ramp amplitude of 25°). During the ramp-hold phase, the UVLM model matches well with small discrepancy compared to all other models. At the final phase (ramp-down), all

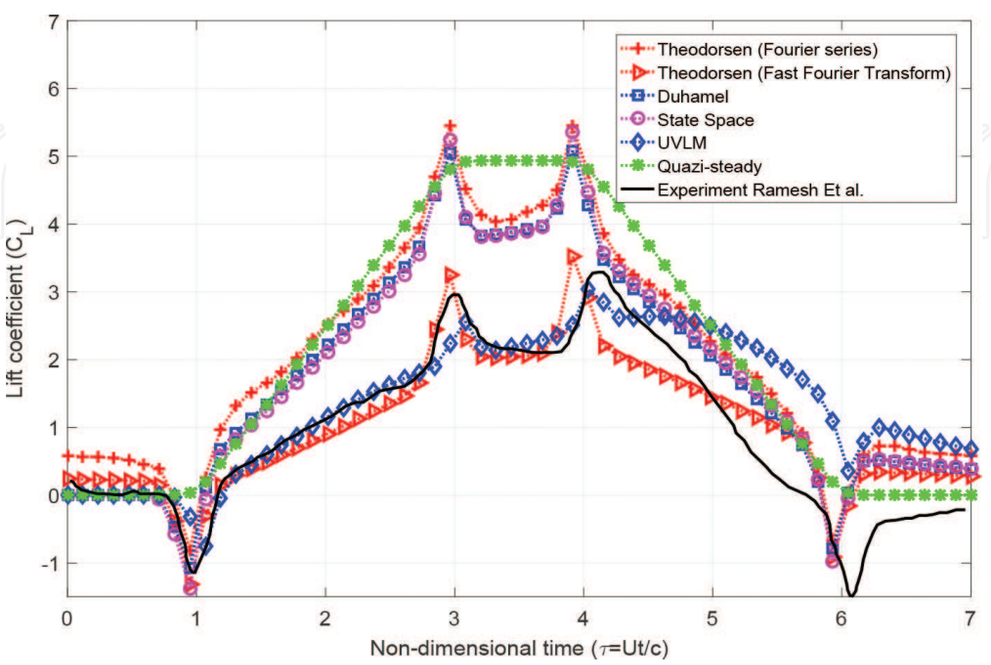

Figure 11.
Comparison for the proposed models and experimental work done by Ramesh et al. with ramp rate of 0.4 and amplitude 45° at trailing pivot location.

models show an over prediction for the lift coefficient. The results show a smooth transition without any sharp peaks in lift coefficient between different events.

4.2.3 Trailing edge pivot

Figure 11 presents the lift coefficient for a ramp amplitude of 45^o at trailing edge pivot location. By comparing **Figure 11** along with **Figure 8**, the two models (Thoedorsen FFT based and UVLM) show a very good prediction with the experimental results for the two phases (ramp-up and ramp hold), then show an increase in the lift coefficient at ramp down. On the contrary, all other models record an over predicted lift coefficient compared to the experimental results for all events preserving the lift response pattern. The quasi steady models for the two ramp cases (0°-25°-0° and 0°-45°-0°) at the same pivot location (trailing edge). **Figure 8** and **Figure 11**, do not show any sharp peak for lift coefficient for the ramp transition regimes. This is expected due to the lack of inclusion of wing stall and rotational effects.

It is clear that a very good matching found between the UVLM model and experiments which can be attributed to the favor of leading edge suction inclusion as well as the nonlinear behavior ($\sin(\alpha)$) that is induced by the no-penetration boundary condition in the UVLM model. Consequently, at this range of AoA (25°) (attached flow), the dominant effect for the LES and nonlinearity associated with the ramp maneuver appears to be matched well with the results of Ramesh et al. [9]. At high angle of attack maneuver (45°), this effect no longer exists as the flow separates and became more pronounced [43]. Recall that rotational lift is proportional to the distance between the pivot and three quarter chord point (Giacomelli and Pistolesi theorem [44]), which attains and preserves its largest value for a leading edge pivot. The UVLM results match the experimental results with small

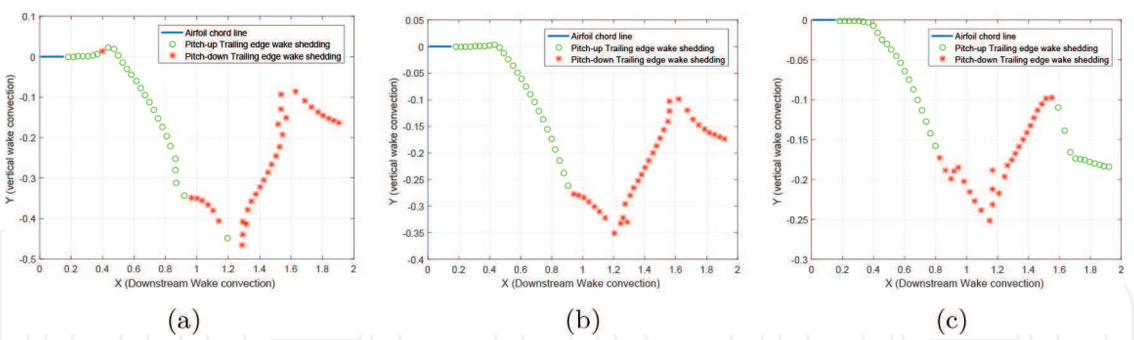

Figure 12.
Shedding of trailing vortices and wake convection downstream for 25° amplitude ramp maneuver. (a) Leading edge pivot. (b) Half chord pivot. (c) Trailing edge pivot.

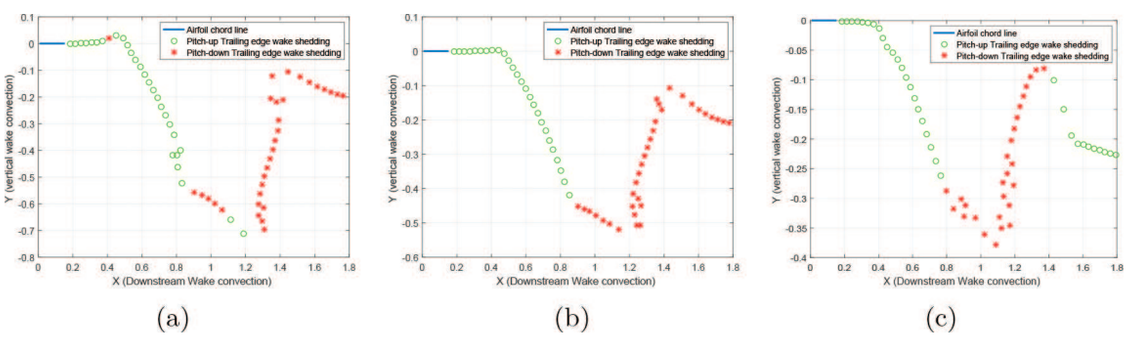

Figure 13.
Shedding of trailing vortices and wake convection downstream for 45° amplitude ramp maneuver. (a) Leading edge pivot. (b) Half chord pivot. (c) Trailing edge pivot.

nuances even for large amplitude (45°) at the ramp-up regime and partially at the ramp-hold only. At ramp-down regime, the UVLM results deviate from the experimental results and appeared to be over predicted.

Figures 12 and **13** show the Shedding of trailing vortices and wake convection shape downstream for 25° and 45° amplitudes ramp maneuvers. All the figures show the same convection pattern for the three pivot locations with an increase in the y axis vortex location with increasing the ramp amplitude.

5. Conclusion

In this chapter, different classical analytical models were presented in a simple mathematical form based on potential flow to solve unsteady problems constrained by an input motion. A canonical pitch ramp motion is chosen to present the input motion for two different ramp amplitudes (25° and 45°) and three pivot location on the airfoil chord ($c/4, c/2, 3c/4$). The analytical results were compared to the experimental data and the comparison revealed an acceptable agreement at the pitch ramp amplitude of 25^o compared to the results presented by the 45^o ramp amplitude case. Thus, those models can be considered as promising aerodynamic models for predicting lift coefficient for such manoeuver at a ramp amplitude up to 25^o only. Along the four analytical models, the UVLM showed very good results for the two ramp amplitude cases. It should be noted that, the UVLM captures all geometric nonlinearities, wake deformation, rolling wake, leading edge suction and post stall without the inclusion of leading edge vortex effects. Duhamel and the state space models appear to have the same behavior which asserts that the state space model shares the same physical base and obtained the same results compared to Theodorsen's model.

Table 2 discuses and concludes the output of each proposed model with the perspective of output response, pitch amplitudes, computational cost and the obtained loads.

The benefits of the UVLM compared to other methods is that is enabling aerodynamic modeling for arbitrary motion. An extension is easy to implement to include a formulation of the boundary conditions for arbitrary three-dimensional motion and control surface rotation. Furthermore the calculation of unsteady induced drag by a nonlinear extension of the force computation can be done. Furthermore the proposed UVLM method shows advantages in predicting unsteady aerodynamic forces of high frequency motion compared to other analytical models. In general, it can be said that the unsteady vortex lattice method is a powerful tool for modeling of incompressible and inviscid unsteady aerodynamics. A continuous time formulation in particular can be used to decrease the computational costs for aeroelastic simulations. The possibility of calculating unsteady loads without the need of approximations for time-domain simulation makes the method especially useful within aeroservoelastic optimization algorithms. Other models formulated in

Models	Response type	Large amplitude	Computational cost	Loads
Theodorsen	Steady state harmonic	×	×	force
Wagner	Transient	×	×	Force
State space	Full response	×	×	Force
UVLM	Full response	√	√	Pressure

Table 2.
Proposed models output parameters for solving pitching maneuvers.

time domain (for example sensor and actuator models or control laws) can be easily integrated. Furthermore, the nonlinear aerodynamic state space formulation is suitable for the integration of further nonlinear aerodynamic correction models (e.g. stall models). This provides confidence towards the development of semi-empirical models based on potential flow theories and experiments that can predict unsteady forces of ramp maneuvers.

Nomenclature

b	airfoil semi-chord $(c/2)$
c	airfoil semi-chord $(c/2)$
C_L	lift coefficient
$C(k)$	lift deficiency factor
f	frequency (Hz)
h	plunging displacement (mm)
$\dot{h}$	plunging velocity
$\ddot{h}$	plunging acceleration
k	reduced frequency $\pi fc/U_\infty$
ℓ	wing span (m)
P	non-dimensional Laplace operator
q	non-dimensional pitch rate,$\frac{\dot{\alpha}c}{V}$
Re	Reynolds number
S	distance traveled in semi-chords,$\frac{2Vt}{c}$
T	time period
U_∞	free stream velocity
U_{rel}	free stream velocity
α_o	airfoil mean angle of attack
α_{eff}	effective angle of attack
$\dot{\alpha}$	angular pitch velocity (rad/s)
$\ddot{\alpha}$	angular pitch acceleration (rad/s^2)

Greek variables

ϕ	phase angle
Γ	total flow circulation
γ_b	elementary bound flow circulation
γ_w	elementary wake flow circulation
ω	angular frequency,(rad/s)
σ	heaviside function variable
τ	Non-dimensional time
ρ	Air density

Abbreviations

AoA	angle of attack
circ	circulatory
FFT	Fast Fourier Transform
RHS	right hand side
UVLM	unsteady vortex lattice method

Author details

Mohamed Yehia Zakaria
Aircraft Mechanics Department, Military Technical College, Cairo, Egypt

*Address all correspondence to: zakaria@mtc.edu.eg

References

[1] Cory, R. and Tedrake, R. (2008). "Experiments in fixed-wing uav perching." *Proceedings of the AIAA Guidance, Navigation, and Control Conference*, AIAA Reston, VA, 1–12.

[2] Hoburg, W. and Tedrake, R. (2009). "System identification of post stall aerodynamics for uav perching." *Proceedings of the AIAA Infotech@ Aerospace Conference*, 1–9. https://en.wikipedia.org/wiki/Swallow, <https://en.wikipedia.org/wiki/Swallow>.

[3] Katz, J. and MASKEW, R. (1988). "Unsteady low-speed aerodynamic model for complete aircraft configurations." *Journal of Aircraft*, 25 (4), 302–310.

[4] Schlichting, H. T. and Truckenbrodt, E. A. (1979). *Aerodynamics of the Airplane*. McGraw-Hill Companies.

[5] Theodorsen, T. and Mutchler, W. (1935). "General theory of aerodynamic instability and the mechanism of flutter.

[6] Yan, Z., Taha, H. E., and Hajj, M. R. (2014). "Geometrically-exact unsteady model for airfoils undergoing large amplitude maneuvers." *Aerospace Science and Technology*.

[7] Theodorsen, T. (1935). "General theory of aerodynamic instability and the mechanism of flutter." *Report No. 496*, NACA.

[8] Zakaria, M. Y., dos Santos, C. R., Dayhoum, A., Marques, F. D., and Hajj, M. R. (2019). "Modeling and prediction of aerodynamic characteristics of free fall rotating wing based on experiments." *IOP Conference Series: Materials Science and Engineering*, 610, 012098.

[9] Roderick, W. R., Cutkosky, M. R., and Lentink, D. (2017). "Touchdown to take-off: at the interface of flight and surface locomotion." *Interface Focus*, 7 (1), 20160094.

[10] Hammer, P., Altman, A., and Eastep, F. (2014). "Validation of a discrete vortex method for low reynolds number unsteady flows." *AIAA journal*, 52(3), 643–649.

[11] Hammer, P., Altman, A., and Eastep, F. (2011). "A discrete vortex method application to high angle of attack maneuvers." *29th AIAA Applied Aerodynamics Conference*, 3007.

[12] Eldredge, J. D., Wang, C., and Ol, M. (2009). "A computational study of a canonical pitch-up, pitch-down wing maneuver." *AIAA paper*, 3687, 2009.

[13] Ramesh, K., Gopalarathnam, A., Edwards, J. R., Ol, M. V., and Granlund, K. (2013). "An unsteady airfoil theory applied to pitching motions validated against experiment and computation.." *Theoretical and Computational Fluid Dynamics*, 1–22.

[14] Yu, Y., Amandolese, X., Fan, C., and Liu, Y. (2018). "Experimental study and modelling of unsteady aerodynamic forces and moment on at plate in high amplitude pitch ramp motion." *Journal of Fluid Mechanics*, 846, 82120.

[15] Pitt Ford, C. and Babinsky, H. (2013). "Lift and the leading-edge vortex." *Journal of Fluid Mechanics*, 720, 280–313.

[16] Shehata, H., Zakaria, M. Y., Hajj, M. R., and Woolsey, C. A. (2019). "Aerodynamic response of a naca-0012 airfoil undergoing non-sinusoidal pitching waveforms." *AIAA Scitech 2019 Forum*, 0303.

[17] Sheng, W., Galbraith, R. M., and Coton, F. (2006). "A new stall-onset criterion for low speed dynamic-stall."

Journal of Solar Energy Engineering, 128 (4), 461–471.

[18] STRGANAC, T. and MOOK, D. (1986). "Application of the unsteady vortex-lattice method to the nonlinear two-degree-of-freedom aeroelastic equations." *27th Structures, Structural Dynamics and Materials Conference*, 867.

[19] Zakaria, M. Y., Al-Haik, M. Y., and Hajj, M. R. (2015). "Experimental analysis of energy harvesting from self-induced flutter of a composite beam." *Applied Physics Letters*, 107(2), 023901.

[20] Zakaria, M. Y. (2018). "Low to medium fidelity models for unsteady pitching maneuvers at low reynolds number." *2018 AIAA Aerospace Sciences Meeting*, 0040.

[21] Dayhoum, A., Zakaria, M. Y., and E. Abdelhamid, O. (2020). "Elastic torsion effects on helicopter rotor loading in forward flight." *AIAA Scitech 2020 Forum*, 0507.

[22] (2019). *Unsteady Aerodynamic Modeling and Prediction of Loads for Rotary Wings in Forward Flight*, Vol. Volume 8: 31st Conference on Mechanical Vibration and Noise of *International Design Engineering Technical Conferences and Computers and Information in Engineering Conference*. V008T10A047.

[23] Michael, V., Altman, A., Eldredge, J. D., Garmann, D. J., and Lian, Y. (2010). "Resume of the aiaa fdtc low reynolds number discussion groups canonical cases.

[24] dos Santos, C. R., Q. Pacheco, D. R., Taha, H. E., and Zakaria, M. Y. (2020). "Nonlinear modeling of electro-aeroelastic dynamics of composite beams with piezoelectric coupling." *Composite Structures*, 112968.

[25] Mook, D. T. and Nayfeh, A. H. (1985). "Application of the vortex-lattice method to high-angle-of-attack subsonic aerodynamics." *SAE Transactions*, 517–532.

[26] Shehata, H., Zakaria, M., Hussein, A., and Hajj, M. R. (2018). "Aerodynamic analysis of flapped airfoil at high angles of attack." *2018 AIAA Aerospace Sciences Meeting*, 0037.

[27] Van der Wall, B. and Leishman, J. G. (1994). "The influence of variable flow velocity on unsteady airfoil behavior." *J. American Helicopter Soc.*, 39(4).

[28] Tietjens, O. K. G. and Prandtl, L. (1957). *Applied hydro-and aeromechanics: based on lectures of L. Prandtl*. Courier Dover Publications.

[29] Garrick, I. E. (1938). "On some reciprocal relations in the theory of nonstationary flows.

[30] Leishman, J. G. and Beddoes, T. S. (1989). "A semi-empirical model for dynamic stall." *J. the American Helicopter Soc.*, 34(3), 3–17.

[31] Marques, F. D., Pereira, D. A., Zakaria, M. Y., and Hajj, M. R. (2017). "Power extraction from stall-induced oscillations of an airfoil." *Journal of Intelligent Material Systems and Structures*, 1045389X17739161.

[32] Wagner, H. (1925). "Uber die entstehung des dynamischen auftriebes von tragugeln." *Zeitschrift fur Angewandte Mathematic und Mechanik*, 35, 17.

[33] M Y Zakaria, D. A. Periera, S. R. M. h. M. D. (2017). "An experimental assessment of unsteady forces on a plunging airfoil oscillating in stationary fluid at high frequencies." *Engineering of Science and Military Technologies Journal*, 1, 13.

[34] M.Y. Zakaria, H.E. Taha, M. H. (2017). "Measurement and modeling of lift enhancement on plunging airfoils: A

frequency response approach." *Journal of Fluids and Structures*, 69(February 2017), Pages–187.

[35] Taha, H. E., Hajj, M. R., and Beran, P. S. (2014). "State-space representation of the unsteady aerodynamics of flapping flight." *Aerospace Science and Technology*, 34, 1–11.

[36] Kussner, H. and Schwartz, I. (1941). "The oscillating wing with aerodynamically balanced elevator.

[37] Katz, J. and Plotkin, A. (2001). *Low Speed Aerodynamics*. Cambridge University Press, 2 edition.

[38] Binder, S., Wildschek, A., and De Breuker, R. "Extension of the continuous time unsteady vortex lattice method for arbitrary motion, control surface deection and induced drag calculation.

[39] Sodja, J., Drazumeric, R., Kosel, T., and Marzocca, P. (2014). "Design of flexible propellers with optimized load-distribution characteristics." *Journal of Aircraft*, 51(1), 117–128.

[40] Konstadinopoulos, P., Thrasher, D., Mook, D., Nayfeh, A., and Watson, L. (1985). "A vortex-lattice method for general, unsteady aerodynamics." *Journal of aircraft*, 22(1), 43–49.

[41] Ramesh, K., Gopalarathnam, A., Edwards, J. R., Ol, M. V., and Granlund, K. (2011). "Theoretical, computational and experimental studies of a at plate undergoing high-amplitude pitching motion." *AIAA Paper*, 217.

[42] Granlund, K. O., Ol, M. V., and Bernal, L. P. (2013). "Unsteady pitching at plates." *Journal of Fluid Mechanics*, 733.

[43] Yu, H.-T., Bernal, L. P., and Morrison, C. (2012). "Experimental investigation of pitch ramp-hold-return motion of at plates at low reynolds number." *AIAA Paper*, 51.

[44] Giacomelli, R. and Pistolesi, E. (1934). "Aerodynamic theory." *Div. D. (ed. Wm. F. Durand). Berlin: Springer*.